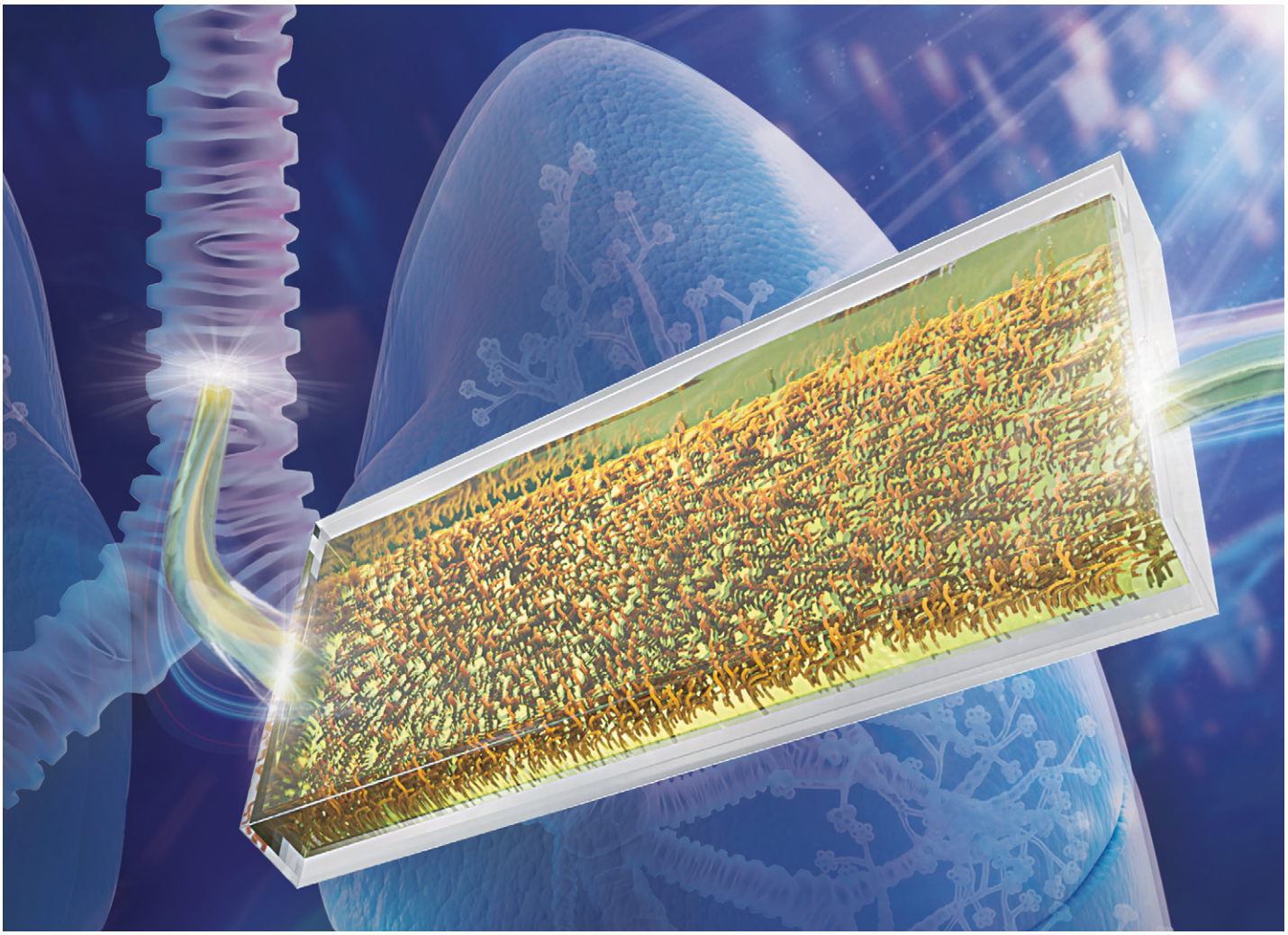

Showcasing research on an *ex vivo* trachea-chip from Professor Yuliang Xie's laboratory, Roy J. Carver Department of Biomedical Engineering, College of Engineering, University of Iowa, Iowa, USA.

Dynamic measurement of airway surface liquid volume with an *ex vivo* trachea-chip

Drs. Yuliang Xie, Paul B. McCray, Jr., and their colleagues incorporated a piece of porcine tracheal explant with a micro-machined device (referred to as "*ex vivo* trachea-chip") to understand the dynamic properties of ASL volume regulation. The *ex vivo* trachea-chip method allows real-time assessment of airway physiology with intact anatomic structures, environmental control, high-resolution, and enhanced experimental throughput.

As featured in:

See Yuliang Xie *et al.*, *Lab Chip*, 2024, **24**, 3093.

ROYAL SOCIETY OF CHEMISTRY

rsc.li/loc

Registered charity number: 207890

Lab on a Chip

PAPER

View Article Online
View Journal | View Issue

Cite this: *Lab Chip*, 2024, **24**, 3093

Dynamic measurement of airway surface liquid volume with an *ex vivo* trachea-chip†

Michael Scott,‡[a] Lei Lei, ‡[b] Kaleb C. Bierstedt, [a] Paul B. McCray Jr.[b] and Yuliang Xie *[a]

Received 9th February 2024,
Accepted 13th May 2024

DOI: 10.1039/d4lc00134f

rsc.li/loc

The volume and composition of airway surface liquid (ASL) is regulated by liquid secretion and absorption across airway epithelia, controlling the pH, solute concentration, and biophysical properties of ASL in health and disease. Here, we developed a method integrating explanted tracheal tissue with a micro-machined device (referred to as "*ex vivo* trachea-chip") to study the dynamic properties of ASL volume regulation. The *ex vivo* trachea-chip allows real-time measurement of ASL transport (J_v) with intact airway anatomic structures, environmental control, high-resolution, and enhanced experimental throughput. Applying this technology to freshly excised tissue we observed ASL absorption under basal conditions. The apical application of amiloride, an inhibitor of airway epithelial sodium channels (ENaC), reduced airway liquid absorption. Furthermore, the basolateral addition of NPPB, a Cl^- channel inhibitor, reduced the basal rate of ASL absorption, implicating a role for basolateral Cl^- channels in ASL volume regulation. When tissues were treated with apical amiloride and basolateral methacholine, a cholinergic agonist that stimulates secretion from airway submucosal glands, the net airway surface liquid production shifted from absorption to secretion. This *ex vivo* trachea-chip provides a new tool to investigate ASL transport dynamics in pulmonary disease states and may aid the development of new therapies targeting ASL regulation.

Introduction

Regulating the volume and composition airway surface liquid (ASL) is critical for pulmonary defense functions.[1] As a thin layer of fluid covering the airway lumen, ASL comprises a mucus-rich layer to trap inhaled pathogens and particulates[2,3] and a periciliary liquid layer that provides a low viscosity environment for ciliary beating.[4] The ASL also contains hundreds of antimicrobial proteins and peptides.[5,6] Alterations in ASL volume caused by environmental (*e.g.*, viral infection,[7] smoking and alcohol[8,9]) or genetic factors (*e.g.*, asthma,[7] cystic fibrosis,[10] and Liddle syndrome[11,12]) impair airway functions. For example, in cystic fibrosis lung disease,[13] abnormal ASL volume[14] changes the biophysical properties of secreted mucins,[15,16] inhibits mucociliary transport,[17] and results in chronic infection and inflammation.[18,19]

In cartilaginous airways (*e.g.*, trachea and bronchi), both airway surface epithelia and submucosal glands contribute to ASL volume regulation through epithelial liquid secretion/absorption.[1,20–22] In ASL secretion, Cl^- enters airway epithelial cells through the basolateral $Na^+/K^+/2Cl^-$ co-transporter (NKCC1)[23] and exits apically *via* CFTR channels.[24] Cl^- secretion drives the movement of water paracellularly[25] or transcellularly,[26] increasing the ASL volume. ASL absorption is a consequence of Na^+ absorption through apical epithelial Na^+ channels (ENaC),[27] followed by the exit of Na^+ *via* the basolateral Na^+/K^+-ATPase.[28] This process drives the movement of Cl^- and water paracellularly[27] or transcellularly,[10] reducing ASL volume. Changes in functions of either airway surface epithelia or submucosal glands impact ASL secretion/absorption, and thereby defense functions.[3] For example, a recent study using genetically modified pigs revealed that a lack of submucosal glands results in changes in ASL composition, reduced ability to kill bacteria, and disrupted mucociliary transport.[29] Given the contributions of epithelia and submucosal glands in ASL secretion/absorption, efforts were made in developing methods to study ASL on intact tissues. For example, Wu *et al.* used flash frozen and fixed bovine airway tissues to study ASL depth.[30] Martens *et al.* weighed ASL collected from bronchial explants stimulated by secretagogues.[31] Welsh *et al.* measured capacitance on the airway surface with an electrode to observe ASL depth.[32] These methods overcame intrinsic limitations of airway cell cultures by

[a] *Roy J. Carver Department of Biomedical Engineering, University of Iowa, USA. E-mail: yuliang-xie@uiowa.edu*
[b] *Stead Family Department of Pediatrics and Pappajohn Biomedical Institute, Roy J. and Lucille A. Carver College of Medicine, University of Iowa, USA*

† Electronic supplementary information (ESI) available. See DOI: https://doi.org/10.1039/d4lc00134f

‡ Authors who contributed equally to this work.

maintaining airway structures (*e.g.*, submucosal glands and epithelia), cell types, and physiological ASL layer; however, the challenges in measuring dynamic changes in ASL volume hinder our understanding ASL physiology.

Integrating a tracheal explant with a micro-machined device as a micro-physiological system (*i.e.*, "*ex vivo* trachea-chip") can be a promising solution to study ASL secretion/absorption. Employing the micro-machined device overcomes technical limitations when using tissue explants. First, the trachea-chip device isolates basolateral and apical surfaces of the airway explants, allowing measurements of secretion- and absorption-dependent liquid transport. The device also enables separate interventions from either the apical or basolateral airway surface. Second, the trachea-chip device exposes and flattens the airway lumen for high resolution microscopic measurement of ASL volume. Third, the micro-physiological system enables not only ASL volume studies but also studies of other physiological processes. In previous studies, we successfully applied the *ex vivo* trachea-chip in studies of mucociliary clearance on the airway surface.[15] In addition to studies of airways, micro-physiological systems[33,34] have been applied to physiological, pharmacological, and toxicological brain research,[35,36] gastrointestinal tract studies,[37–39] and liver investigations.[40,41]

In this work, we employ an *ex vivo* trachea-chip strategy to study the dynamic changes in ASL volume on the surface of newborn pig trachea. We investigate the effects of 5-nitro-2(3-phenylpropylamino) benzoic acid (NPPB, applied basolaterally to inhibit Cl^- channels), amiloride (an inhibitor of apical Na^+ channels), and methacholine (a submucosal gland secretagogue). We also analyze factors that impact ASL homeostasis, discuss the technical advantages and limitations of *ex vivo* trachea-chip, and provide our perspectives on future directions.

Methods

Chemicals

Fluorescent saline (containing 137.8 mM NaCl, 4 mM KCl, 29 mM $NaHCO_3$, 1.2 mM $CaCl_2$, 0.6 mM $MgCl_2$, 1 mM NaH_2PO_4, 17.5 mM fluorescein, pH 7.4) was used to study the ASL secretion and absorption.[42] Krebs-Ringer buffer (containing 118.9 mM NaCl, 25 mM $NaHCO_3$, 10 mM dextrose, 2.4 mM K_2HPO_4, 0.6 mM KH_2PO_4, 1.2 mM $CaCl_2$, 1.2 mM $MgCl_2$, pH = 7.4 with 5% CO_2) was used for basolateral perfusion. In some experiments, 5-nitro-2(3-phenylpropylamino) benzoic acid (Sigma Aldrich, USA), methacholine (Sigma Aldrich, USA), or amiloride (Sigma Aldrich, USA) were used as interventions.

Animals

The University of Iowa Animal Care and Use Committee (IACUC) approved all animal studies. Wildtype pigs were obtained from Exemplar Genetics and Premier BioSource. Tracheal tissues were harvested within 24 hours after birth. Animals were anesthetized with ketamine (20 mg kg^{-1}, I.M.) (Phoenix Pharmaceutical, Inc., USA) and xylazine (2 mg kg^{-1}, I.M.) (Lloyd, USA). Euthanasia was conducted with Euthasol (Virbac, France) intravenously. To harvest tissue, a tracheal segment between the opening of the right cranial lobe and the larynx was transected with a surgical blade between cartilage rings and removed. The tracheal segments were immediately placed in a sealed centrifuge tube, on a PBS-soaked surgical gauze, and stored at 4 °C for less than 24 hours before experiments.

Design of *ex vivo* trachea-chip

A tracheal segment (length of ~1 cm) was opened with a longitudinal incision on the ventral aspect (Fig. 1A and B). The thickness of tracheal tissue is about 1 mm (Fig. S1†). The opened tracheal explant was mounted onto a device that separates the apical and basolateral surfaces of the trachea (*i.e.*, trachea-chip) (Fig. 1C). The device is made of aluminum, designed using Cero software (PTC, MA, USA), and manufactured through computer numerical controlled machining (Protolabs, MN, USA). The trachea-chip device consists of three parts (Fig. 1D), *i.e.*, a top part that features an apical chamber with dimensions of 8 mm (length) by 5 mm (width) by 3 mm (depth) to accommodate ASL; a bottom part containing a basolateral perfusion chamber with dimensions of 8 mm (length) by 5 mm (width) by 3 mm (depth); and a metal mesh inserted into the bottom part to prevent tracheal tissue deformation. The top and bottom parts were aligned onto an optical breadboard with screws (Thorlabs, NJ, USA). After sandwiching a tracheal explant between the apical and basolateral chambers (Fig. 1D), the trachea-chip assembly was mounted in an environmental chamber with 5% CO_2 and 100% saturated humidity at 37 °C (Fig. 1E and F). 50 μL of fluorescent saline was added to the apical chamber, followed by the apical addition of ~50 μL mineral oil to fill the apical chamber. The basolateral side of trachea was perfused with Krebs-Ringer buffer through the built-in channels (Fig. 1D). The Krebs-Ringer perfusion buffer was continuously oxygenated by bubbling with air with 5% CO_2. The perfusion flow rate was maintained at 60 μL min^{-1} with syringe pumps (neMESYS, Cetoni GmbH, Germany). At this perfusion rate, the basolateral solution turns over every 2 min.

Visualization of ASL volume

The images of fluorescent ASL were obtained using an upright confocal microscope (A1R, Nikon, USA) using a 10× objective (NA = 0.45). In the *XY*-direction, the area of ASL analyzed is 1.62 mm^2 (*i.e.*, 1.27 mm by 1.27 mm). To study the volume of ASL, a *Z*-direction scanning (with a *Z*-step of 5 μm) was applied, starting from below the airway surface until above the mineral oil. The ASL volume was calculated using Imaris software (Oxford Instruments, UK). To capture changes in ASL across the entire explant, we imaged the tracheal surface at 3 different positions using an automated stage controller (MS-2000-500, Applied Scientific Instrumentation, OR, USA). To measure dynamic changes in ASL volume the imaging procedure was conducted at multiple time points with a minimum interval of 15 min.

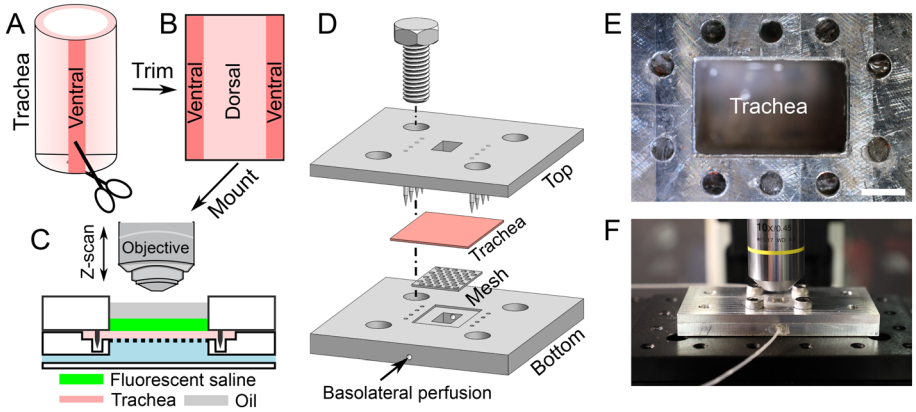

Fig. 1 The *ex vivo* trachea-chip device to measure ASL secretion/absorption is demonstrated schematically. (A–C) Procedures to dissect tracheal tissue and mount it in the device to study ASL volume. (D) 3D drawing of the *ex vivo* trachea-chip device comprised of a top plate, a tracheal explant, a metal mesh, and a bottom plate with perfusion ports. (E and F) Photos of assembled *ex vivo* trachea-chip device on a confocal microscope stage. Scale bar is 2 mm.

Volumetric flow rate of ASL secretion/absorption (J_v)

The volumetric flow rate of ASL secretion/absorption (J_v)[43] is calculated by eqn (1),

$$J_v\ (\mu L\ cm^{-2}\ h^{-1}) = (V_t - V_0)/A/t \quad (1)$$

where V_0 and V_t are ASL volume measured at time 0 and t hours, respectively. A is the area of ASL that was scanned; in this study A = 1.62 mm^2. A positive J_v indicates ASL secretion and a negative J_v indicates ASL absorption. Three positions on each tracheal surface were averaged, 5–6 biological replicates were used in the experiments.

The experimental results were analyzed with Prism software (GraphPad Software, MA, USA). Most data were represented as mean ± standard error of mean (SEM) unless otherwise stated. Paired or un-paired t-tests were used to compare the results. $p < 0.05$ was considered statistically significant.

Results

The volume of ASL is assessed on the surface of a trachea explant

Computational reconstruction of stacked images, captured using a confocal microscope, was used to assess the volume of ASL (Fig. 2A). At Z-positions from the closest to the most

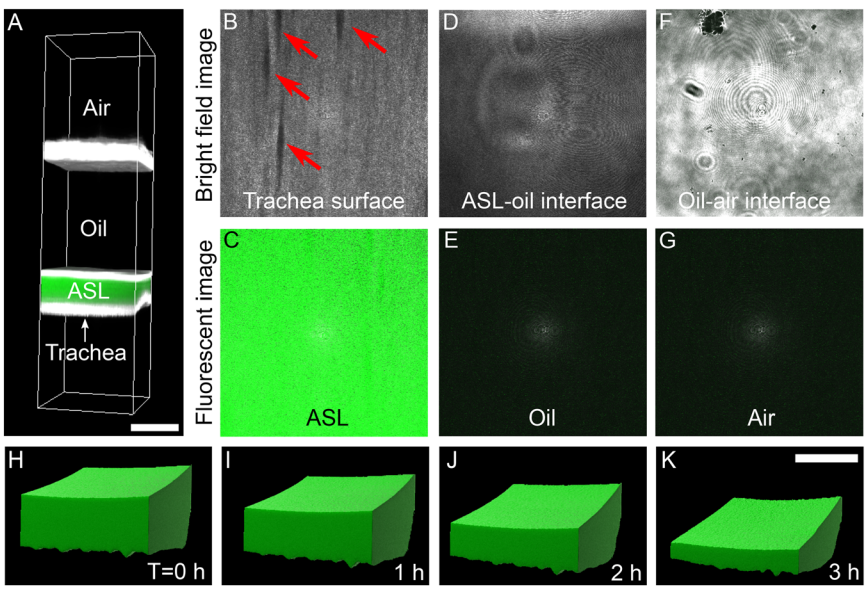

Fig. 2 Quantification of dynamic changes in ASL volume using confocal microscopy. (A) Stacked images along Z-direction at the apical surface of trachea explant. (B–G) Representative images at different Z positions, from the closest to most distal from the airway surface, including the airway surface (B, red arrows point to submucosal gland ducts), fluorescent ASL (C), aqueous–oil interface (D), oil (E), oil–air interface (F), and air (G), where (B, D, and E) are bright field images, and (C, E and G) are fluorescent images. (H–K) Computational reconstruction of ASL volume at indicated time points. Scale bar is 1 mm.

distant from the airway surface, we progressively observed the trachea surface with ducts of submucosal glands (arrows in Fig. 2B), fluorescent ASL (Fig. 2C), ASL-oil interface (Fig. 2D), non-fluorescent oil (Fig. 2E), oil-air interface (Fig. 2F), and air (Fig. 2G). Clear boundaries between trachea surface, fluorescent ASL, mineral oil was observed to identify the volume of ASL. Imaris software were used to reconstruct the ASL volume (Fig. 2H–K). The changes in ASL volume were measured at multiple time points. For example, with basolateral perfusion of Krebs buffer over a period of 3 hours, we found that the ASL volume decreased (Fig. 2H–K), indicating that airways are absorbing ASL at baseline.

Apical application of amiloride reduces the rate of ASL absorption

We first studied the changes in ASL volume under basal conditions and following the apical addition of amiloride (10 μM), an inhibitor of epithelial sodium channels (ENaC).[44] The basolateral surface was continuously perfused with Krebs buffer during the experiment. We observed that the apical addition of amiloride inhibited ASL absorption during a 30 min period (Fig. 3A). The rate of ASL secretion and absorption (J_v) was further calculated using eqn (1). The J_v became less negative compared with donor matched untreated pig trachea (p = 0.0788) (Fig. 3B), revealing a reduced rate of ASL absorption. Of note, the measured J_v was greater than, but in the same order of previous measurements made using cultured airway epithelial cells, suggesting a similar basal absorptive function in both cultured airway epithelial cells and tissue explants. For example, Zabner *et al.* reported an ASL absorption rate of approximately 5 μL cm^{-2} h^{-1} using primary cultures of well differentiated human airway epithelial cells.[42]

Basolateral perfusion with methacholine does not significantly alter ASL absorption

In previous studies, we showed that basolateral perfusion of methacholine stimulates liquid secretion from submucosal glands.[15] To evaluate the impact of methacholine on ASL homeostasis, we added methacholine to the basolateral perfusate. Perfusion with methacholine (2.5 μg mL^{-1}) began 15 min before the first recording of ASL volume and continued until the end of experiment, and volumes of ASL were recorded every 15 min (Fig. 3C). We found that methacholine perfusion did not significantly change the J_v (p = 0.2608) when comparing to the no methacholine group over a 30 min period (Fig. 3D). This result is consistent with previous ASL depth measurement on frozen bovine airways, where methacholine only increases the ASL height transiently.[30] However, in our previous study, we showed that methacholine stimulates submucosal glands secretion.[15] We speculate that when submucosal gland secretion is stimulated by methacholine, increased ASL absorption by surface epithelia occurred

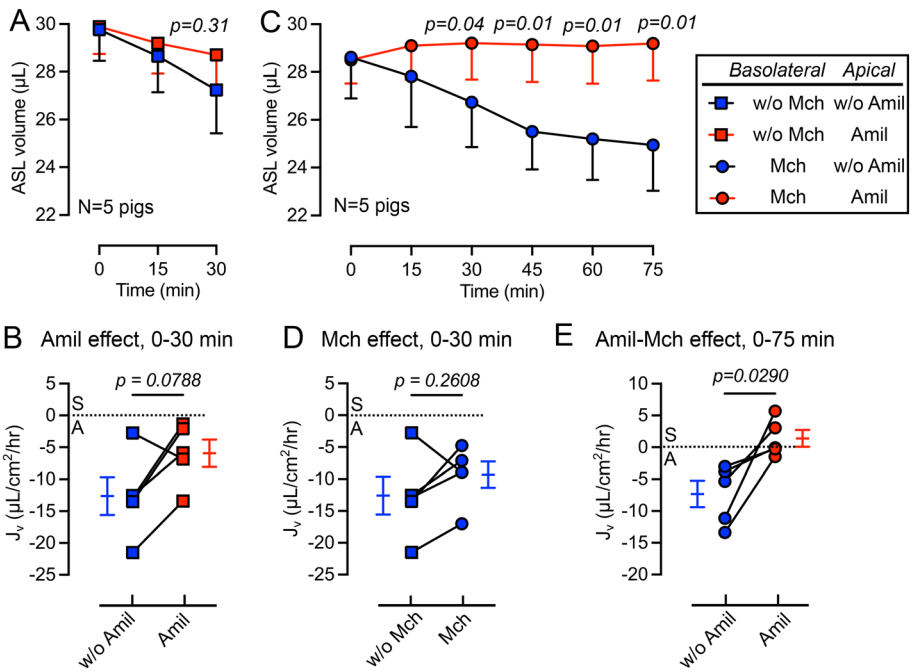

Fig. 3 Addition of apical amiloride and/or basolateral methacholine impacts ASL absorption and secretion. (A) Changes in ASL volume in response to apical amiloride (Amil, 10 μM) over a 30 min observation. (B) The effect of apical amiloride on volumetric rate of ASL secretion or absorption (J_v), where "S" means secretion and "A" means absorption. (C) Changes in ASL volume in response to the addition of basolateral methacholine (Mch, 2.5 μg mL^{-1}) and apical amiloride (Amil, 10 μM) over a 75 min observation period. (D) The effect of basolateral methacholine on volumetric rate of ASL secretion/absorption (J_v). (E) The effect of apical amiloride combined with basolateral methacholine on the volumetric rate of ASL secretion/absorption (J_v). Positive J_v numbers represent ASL secretion and negative J_v numbers represent ASL absorption. Data are presented as mean and SEM, compared using paired t-tests, n = tracheal tissues from 5 pigs.

simultaneously to maintain a balance between ASL secretion and absorption.

The combined addition of apical amiloride and basolateral methacholine shifts J_v from absorption to secretion

To further modify the balance between ASL secretion and absorption, we added amiloride (10 μM) to the apical surface in combination with basolateral methacholine (2.5 μg mL^{-1}) perfusion. This combination increased the volume of ASL on the trachea surface (red in Fig. 3C), confirmed by a positive J_v value (Fig. 3E). We speculate that this shift from ASL absorption to secretion is mediated by inhibition of ENaC in surface epithelia by apical amiloride and methacholine stimulation of submucosal gland liquid secretion. Together, this increases the ASL volume. However, if apical amiloride enters submucosal glands, it may also inhibit liquid absorption and increase ASL volume. Previous studies showed that small molecules with molecular weights similar to amiloride can reach submucosal glands when applied to the airway surface.[45]

Basolateral perfusion with NPPB reduces the rate of ASL absorption

Previous studies provided evidence of basolateral Cl^- channels in airway epithelia that may contribute to transepithelial electrolyte and liquid transport.[46–49] For example, using cultured bovine tracheal epithelia Uyekubo *et al.* found that basolateral Cl^- conductance and transepithelial liquid absorption was inhibited by 5-nitro-2(3-phenylpropylamino) benzoic acid (NPPB).[50] To understand the role of basolateral Cl^- channels on airway organ explants, we perfused NPPB (100 μM) through the basolateral chamber. During the 3-hour experimental time, the cilia beating frequency does not change significantly, suggesting that tissue remains viable (Fig. S2†). The basolateral perfusion of NPPB resulted a greater ASL volume remaining on the airway surface over a 3-hour time course (Fig. 4A). The calculation of J_v revealed that NPPB induced a significant (p = 0.003) decrease in the rate of ASL absorption compared to controls (Fig. 4B). This result in intact tissue is consistent with a recent report in cultured epithelial cells demonstrating the presence of basolateral barttin/Cl^- channels that help mediate liquid absorption.[10] NPPB has been previously demonstrated to inhibit barttin/Cl^- channels.[46–49]

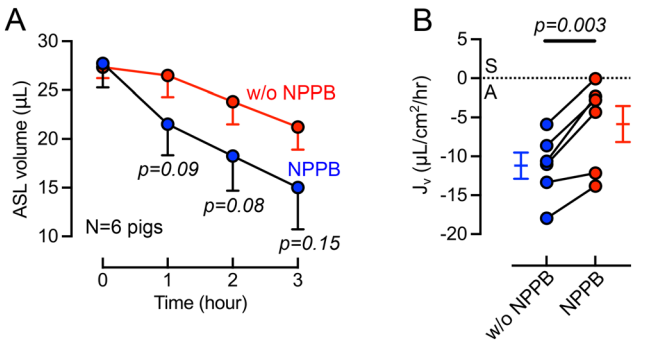

Fig. 4 Basolateral perfusion of 5-nitro-2(3-phenylpropylamino) benzoic acid (NPPB) reduces the rate of ASL absorption. (A) Changes in ASL volume in response to basolateral addition of NPPB (10 μM) over a 3-hour period. (B) Effect of basolateral NPPB perfusion on J_v over a 3-hours interval. Positive J_v numbers represent ASL secretion and negative numbers represent ASL absorption. Data are presented as mean and SEM, compared using paired *t*-tests, *n* = tracheal tissues from 6 pigs.

The trachea explant from pigs used in this work shares many similarities to human airways and are applicable to future studies on pig models with airway diseases. Studies in pig models of airway diseases, *e.g.*, cystic fibrosis,[53,54] and ectodysplasin null pigs lacking submucosal glands,[29] have contributed to knowledge of airway defenses and disease pathogenesis. The *ex vivo* trachea-chip strategy can be readily applied to tissues from other species, including human samples.

The on-chip strategy simplifies dynamic observation, intervention, and reduces tissue consumption. The *ex vivo* trachea-chip design allows direct observation of ASL volume with a standard confocal microscope (Fig. 2) and a temporal resolution in minutes and spatial resolution in <10 μm. Direct observation of ASL volume does not require use of flash frozen tissue,[30] capacitance measurements,[32,55] or collection and weighing of ASL.[31] The on-chip strategy also enables interventions to modify airway physiology. The top and bottom chambers allow separate interventions to the apical and basolateral tracheal surfaces, exemplified by the methacholine and amiloride experiments (Fig. 3). In addition, the *ex vivo* trachea-chip approach requires a piece of trachea tissue ~1 cm in length (Fig. 1). Owing to the reduced tissue consumption, multiple samples can be derived from a single animal or human donor, providing the opportunity to compare drug effects with the most accurate background.

Discussion

Advantages of *ex vivo* trachea-chip in studying ASL dynamics

The *ex vivo* organ explant maintains tracheal anatomic structures and cell types, which closely recapitulates *in vivo* physiology. For example, submucosal glands in cartilaginous airways (*e.g.*, trachea and major bronchi) are a major source of ASL secretion;[51,52] however, previous ASL studies with cultured epithelial cells lack the contributions from submucosal glands. The use of a tracheal explant allows us to study the contributions from both surface epithelia and submucosal glands to ASL secretion and absorption.

Factors that impact ASL volume and J_v

Our studies confirm earlier work using cultured airway epithelia indicating that airway epithelia are a major site for liquid absorption.[10,24,42] We found a baseline absorption rate of ~10 μL cm^{-2} h^{-1} (Fig. 3B); in comparison, the ASL absorption rate measured using cultured human airway epithelial cells was ~5 μL cm^{-2} h^{-1}.[42] Despite several experimental differences in the models (*e.g.*, species, media used in basolateral perfusion, and methods of ASL volume measurement), the J_v results are within the same order of magnitude. In contrast, earlier studies

demonstrated that submucosal glands are a major site of liquid secretion in the cartilaginous airways.[15,56–58] We also observed that addition of the cholinergic agonist methacholine[15,17] failed to significantly change the rate of absorption (Fig. 3D). However, the combination of submucosal gland stimulation with methacholine and inhibition of surface epithelia with amiloride shifted J_v from net absorption to secretion (Fig. 3E). This result may have therapeutic implications for airway diseases associated with impaired liquid secretion, such as cystic fibrosis.[14] To further identify contributions from submucosal glands and epithelia in ASL regulation a pig model lacking submucosal glands was recently reported.[29]

The observed effect of the basolateral addition of NPPB suggests that basolateral Cl^- channels contribute to transepithelial liquid transport across the airways. In bovine tracheal epithelia, Uyekubo *et al.* identified a NPPB inhibited basolateral Cl^- conductance involved in transepithelial liquid absorption.[50] Using well-differentiated human airway epithelia, Itani *et al.* discovered a basolateral 4,4-diisothiocyanostilbene-2,2-disulfonic acid (DIDS)-sensitive Cl^- channel that was activated by cyclic adenosine monophosphate (cAMP), protein kinase C, and a reduction in pH.[46] In Calu-3 cells, Linsdell *et al.* described the expression of Cl^- voltage-gated channels (ClC-Ka and ClC-Kb), and barttin CLCNK-Type Cl^- channel accessory beta subunit (BSND) protein.[59] We recently reported that pulmonary ionocytes express basolateral CLCNKB/BSND channels that mediate Cl^- transport and liquid absorption.[10] In this study, the *ex vivo* trachea-chip device allowed basolateral perfusion with NPPB to inhibit basolateral Cl^- channels, including CLCNKB/BSND channels, revealing their physiological role in maintaining ASL volume in intact tracheal tissue. We acknowledge that NPPB can inhibit other channels, including CFTR, and other intracellular targets.

Current limitations and future directions

As a first-of-the-kind study, the current work also has limitations. First, current study of ASL absorption/secretion is limited by its temporal and spatial resolution. We measured the secretion and absorption of external liquid added onto the airway surfaces. Adding liquid facilitates observation of changes in ASL volume and simplifies the procedure for adding apical interventions (*e.g.*, amiloride); however, it may perturb the regulation of native ASL. In future studies, the use of an objective with a larger numerical aperture could be employed to study changes in the volume of native ASL (with a depth of 10–15 μm).[60,61] The temporal resolution of ASL dynamics can also be improved. In this work, we used a 15 min interval between measurements. These time intervals could miss transient events in ASL secretion or absorption. For example, previous studies using flash freezing of bovine trachea suggested a transient increase in ASL volume within 2 min of methacholine treatment, and a return to baseline within 5 min.[30] In the future, a microscope with faster scanning rate could be used to improve temporal resolution.

In this work we used newborn, wildtype pig airway explants, and did not employ organ explants from disease animal models or human donors. Experiments using neonatal tissues from disease models allows studies at the time of onset of airway disease, while tissues from human donors may allow us to study ASL dynamics in more advanced airway diseases (*e.g.*, severe viral/bacterial infection, fatal asthma). Using cultures airway epithelial cells, previous studies found that bacterial infection changes ASL composition,[62] and exposure to inflammatory cytokines (*e.g.*, TNF-α/IL-17) changes both ASL height and pH;[18] genetic factors, such as CFTR mutations, change ASL height, pH, and viscosity.[63,64] Future studies with tissues from other animal models of diseases (*e.g.*, pig and ferret model of cystic fibrosis[65,66]) and human airway explants could address questions regarding how disease states impact ASL secretion and absorption at the organ level.

Future studies would also benefit from further device innovation. We believe that with device miniaturization, the system could be adapted to study smaller caliber airways (such as from mice), or from dissected small airways from large animal models and human lung tissues. In addition, the current trachea-chip is low throughput (*i.e.*, approximated 5 pieces of tissue can be obtained from a newborn pig trachea). We expect that a micro-fluidic channel design and precise tissue segments would enable airway tissue-chips with enhanced throughput.

Conclusion

In this work, we developed an *ex vivo* trachea-chip strategy to study the dynamics of ASL secretion and absorption. This *ex vivo* trachea-chip allows use of whole organ with intact anatomic structures, visualization with high resolution, facile intervention of airway physiology, and improved throughput. The trachea-chip device sandwiches a piece of organ explant that was opened and flattened; the volume of ASL is assessed through confocal images of fluorescent liquid under the cover of mineral oil. Chemicals (*e.g.*, amiloride, methacholine, and NPPB) were applied either basolaterally or apically to impact the ASL dynamics. On newborn pig tracheal tissue, we observed that apical addition of amiloride and basolateral addition of NPPB decreased the ASL absorption rate while the combined application of apical amiloride and basolateral methacholine shifted J_v from absorption to secretion. These results demonstrate the utility of the *ex vivo* trachea-chip strategy as a new tool to investigate ASL transport in pulmonary physiology and may aid the development of new therapies targeting ASL regulation.

Author contributions

PM and YX conceptualized the project. MS designed and fabricated device. LL, MS, and KB conducted experiments and interpreted the data. YX wrote the initial draft of the paper and all authors contributed to the writing.

Conflicts of interest

The authors declare no competing interests.

Acknowledgements

This research is supported by Carver Faculty Start-Up Funds, National Heart, Lung, and Blood Institute, R21HL161499, National Institute of Biomedical Imaging and Bioengineering R01EB033395, and Cystic Fibrosis Foundation 003140I221 to Y. X. Also supported by National Heart, Lung, and Blood Institute P01HL152960 to P. M. P. M. is supported by the Roy J. Carver Charitable Trust.

References

1 R. C. Boucher, Molecular insights into the physiology of the 'thin film' of airway surface liquid, *J. Physiol.*, 1999, **516**(3), 631–638.
2 J. H. Widdicombe and J. G. Widdicombe, Regulation of human airway surface liquid, *Respir. Physiol.*, 1995, **99**(1), 3–12.
3 J. V. Fahy and B. F. Dickey, Airway mucus function and dysfunction, *N. Engl. J. Med.*, 2010, **363**(23), 2233–2247.
4 B. Button, *et al.*, A periciliary brush promotes the lung health by separating the mucus layer from airway epithelia, *Science*, 2012, **337**(6097), 937–941.
5 J. M. Jacobs, *et al.*, Proteomic Analysis of Pure Human Airway Gland Mucus Reveals a Large Component of Protective Proteins, *PLoS One*, 2015, **10**(2), e0116756.
6 J. A. Bartlett, *et al.*, Protein composition of bronchoalveolar lavage fluid and airway surface liquid from newborn pigs, *Am. J. Physiol.*, 2013, **305**(3), L256–L266.
7 Y. Nakagami, *et al.*, The epithelial anion transporter pendrin is induced by allergy and rhinovirus infection, regulates airway surface liquid, and increases airway reactivity and inflammation in an asthma model, *J. Immunol.*, 2008, **181**(3), 2203–2210.
8 J. Tyrrell, *et al.*, Evaluation of chronic cigarette smoke exposure in human bronchial epithelial cultures, *J. Appl. Toxicol.*, 2023, **43**(6), 862–873.
9 L. Rasmussen, *et al.*, Alcohol-Induced Mucociliary Dysfunction: Role of Defective CFTR Channel Function, *bioRxiv*, 2023, preprint, DOI: 10.1101/2023.07.17.548927.
10 L. Lei, *et al.*, CFTR-rich ionocytes mediate chloride absorption across airway epithelia, *J. Clin. Invest.*, 2023, **133**(20), e171268.
11 M. A. Mall, *et al.*, Airway surface liquid volume regulation determines different airway phenotypes in liddle compared with betaENaC-overexpressing mice, *J. Biol. Chem.*, 2010, **285**(35), 26945–26955.
12 D. Rotin and O. Staub, Function and Regulation of the Epithelial Na(+) Channel ENaC, *Compr. Physiol.*, 2021, **11**(3), 2017–2045.
13 D. A. Stoltz, D. K. Meyerholz and M. J. Welsh, Origins of cystic fibrosis lung disease, *N. Engl. J. Med.*, 2015, **372**(4), 351–362.
14 R. C. Boucher, Airway surface dehydration in cystic fibrosis: pathogenesis and therapy, *Annu. Rev. Med.*, 2007, **58**, 157–170.
15 Y. Xie, *et al.*, Acidic submucosal gland pH and elevated protein concentration produce abnormal cystic fibrosis mucus, *Dev. Cell*, 2020, **54**(4), 488–500.e5.
16 T. Kato, *et al.*, Mucus concentration-dependent biophysical abnormalities unify submucosal gland and superficial airway dysfunction in cystic fibrosis, *Sci. Adv.*, 2022, **8**(13), eabm9718.
17 M. J. Hoegger, *et al.*, Impaired mucus detachment disrupts mucociliary transport in a piglet model of cystic fibrosis, *Science*, 2014, **345**(6198), 818.
18 T. Rehman, *et al.*, Inflammatory cytokines TNF-alpha and IL-17 enhance the efficacy of cystic fibrosis transmembrane conductance regulator modulators, *J. Clin. Invest.*, 2021, **131**(16), e150398.
19 T. Rehman and M. J. Welsh, Inflammation as a Regulator of the Airway Surface Liquid pH in Cystic Fibrosis, *Cells*, 2023, **12**(8), 1104.
20 R. C. Boucher, Regulation of airway surface liquid volume by human airway epithelia, *Pflugers Arch*, 2003, **445**(4), 495–498.
21 R. Tarran, Regulation of airway surface liquid volume and mucus transport by active ion transport, *Proc. Am. Thorac. Soc.*, 2004, **1**(1), 42–46.
22 J. H. Widdicombe, *et al.*, Regulation of depth and composition of airway surface liquid, *Eur. Respir. J.*, 1997, **10**(12), 2892–2897.
23 D. J. Gillie, *et al.*, Liquid and ion transport by fetal airway and lung epithelia of mice deficient in sodium-potassium-2-chloride transporter, *Am. J. Respir. Cell Mol. Biol.*, 2001, **25**(1), 14–20.
24 J. J. Smith, P. H. Karp and M. J. Welsh, Defective fluid transport by cystic fibrosis airway epithelia, *J. Clin. Invest.*, 1994, **93**(3), 1307–1311.
25 J. A. Reihill, L. E. J. Douglas and S. L. Martin, Modulation of Ion Transport to Restore Airway Hydration in Cystic Fibrosis, *Genes*, 2021, **12**(3), 453.
26 A. S. Verkman, Role of aquaporins in lung liquid physiology, *Respir. Physiol. Neurobiol.*, 2007, **159**(3), 324–330.
27 D. V. Olivenca, *et al.*, Thickness of the airway surface liquid layer in the lung is affected in cystic fibrosis by compromised synergistic regulation of the ENaC ion channel, *J. R. Soc., Interface*, 2019, **16**(157), 20190187.
28 P. Factor, Role and regulation of lung Na,K-ATPase, *Cell. Mol. Biol.*, 2001, **47**(2), 347–361.
29 L. S. Ostedgaard, *et al.*, Lack of airway submucosal glands impairs respiratory host defenses, *Elife*, 2020, **9**, e59653.
30 D. X. Wu, *et al.*, Regulation of the depth of surface liquid in bovine trachea, *Am. J. Physiol.*, 1998, **274**(3), L388–L395.
31 C. J. Martens and S. T. Ballard, Effects of secretagogues on net and unidirectional liquid fluxes across porcine bronchial airways, *Am. J. Physiol.*, 2010, **298**(2), L270–L276.
32 M. J. Welsh, J. H. Widdicombe and J. A. Nadel, Fluid transport across the canine tracheal epithelium, *J. Appl. Physiol.: Respir., Environ. Exercise Physiol.*, 1980, **49**(5), 905–909.
33 J. P. Wikswo, The relevance and potential roles of microphysiological systems in biology and medicine, *Exp. Biol. Med.*, 2014, **239**(9), 1061–1072.

34 F. C. Garcia-Garcia, *et al.*, Microfluidic technologies for *ex vivo* tissue biopsies: A review, *Organs-on-a-Chip*, 2022, **4**, 100020.
35 Y. Huang, J. C. Williams and S. M. Johnson, Brain slice on a chip: opportunities and challenges of applying microfluidic technology to intact tissues, *Lab Chip*, 2012, **12**(12), 2103–2117.
36 A. J. Blake, *et al.*, Multilayer PDMS microfluidic chamber for controlling brain slice microenvironment, *Lab Chip*, 2007, **7**(7), 842–849.
37 H. Eslami Amirabadi, *et al.*, Intestinal explant barrier chip: long-term intestinal absorption screening in a novel microphysiological system using tissue explants, *Lab Chip*, 2022, **22**(2), 326–342.
38 A. Richardson, *et al.*, A microfluidic organotypic device for culture of mammalian intestinesex vivo, *Anal. Methods*, 2020, **12**(3), 297–303.
39 A. Dawson, *et al.*, A microfluidic chip based model for the study of full thickness human intestinal tissue using dual flow, *Biomicrofluidics*, 2016, **10**(6), 064101.
40 K. Schumacher, *et al.*, Perfusion Culture Improves the Maintenance of Cultured Liver Tissue Slices, *Tissue Eng.*, 2007, **13**(1), 197–205.
41 I. A. M. de Graaf, *et al.*, Preparation and incubation of precision-cut liver and intestinal slices for application in drug metabolism and toxicity studies, *Nat. Protoc.*, 2010, **5**(9), 1540–1551.
42 J. Zabner, *et al.*, Loss of CFTR chloride channels alters salt absorption by cystic fibrosis airway epithelia in vitro, *Mol. Cell*, 1998, **2**(3), 397–403.
43 G. Wiedner, Method to detect volume flows in the nanoliter range, *Rev. Sci. Instrum.*, 1976, **47**(6), 775–776.
44 C. M. Canessa, *et al.*, Amiloride-sensitive epithelial Na+ channel is made of three homologous subunits, *Nature*, 1994, **367**(6462), 463–467.
45 W. Yu, *et al.*, Pulmonary neuroendocrine cells sense succinate to stimulate myoepithelial cell contraction, *Dev. Cell*, 2022, **57**(18), 2221–2236.e5.
46 O. A. Itani, *et al.*, Basolateral chloride current in human airway epithelia, *Am. J. Physiol.*, 2007, **293**(4), L991–L999.
47 W. C. Valinsky, R. M. Touyz and A. Shrier, Characterization of constitutive and acid-induced outwardly rectifying chloride currents in immortalized mouse distal tubular cells, *Biochim. Biophys. Acta, Gen. Subj.*, 2017, **1861**(8), 2007–2019.
48 S. L'Hoste, *et al.*, Characterization of the mouse ClC-K1/Barttin chloride channel, *Biochim. Biophys. Acta*, 2013, **1828**(11), 2399–2409.
49 A. Liantonio, *et al.*, Investigations of pharmacologic properties of the renal CLC-K1 chloride channel co-expressed with barttin by the use of 2-(p-Chlorophenoxy) propionic acid derivatives and other structurally unrelated chloride channels blockers, *J. Am. Soc. Nephrol.*, 2004, **15**(1), 13–20.
50 S. N. Uyekubo, *et al.*, cAMP-dependent absorption of chloride across airway epithelium, *Am. J. Physiol.*, 1998, **275**(6), L1219–L1227.
51 J. E. Phillips, J. A. Hey and M. R. Corboz, Effects of ion transport inhibitors on MCh-mediated secretion from porcine airway submucosal glands, *J. Appl. Physiol.*, 2002, **93**(3), 873–881.
52 J. Chen and C. X. Bai, The relationship between aquaporin water channels and fluid secretion in airway submucosal glands, *Zhonghua Jiehe He Huxi Zazhi*, 2003, **26**(8), 485–487.
53 C. S. Rogers, *et al.*, Disruption of the CFTR gene produces a model of cystic fibrosis in newborn pigs, *Science*, 2008, **321**(5897), 1837–1841.
54 L. S. Ostedgaard, *et al.*, The DeltaF508 mutation causes CFTR misprocessing and cystic fibrosis-like disease in pigs, *Sci. Transl. Med.*, 2011, **3**(74), 74ra24.
55 C. Jiang, *et al.*, Altered fluid transport across airway epithelium in cystic fibrosis, *Science*, 1993, **262**(5132), 424–427.
56 H. J. Cho, N. S. Joo and J. J. Wine, Defective fluid secretion from submucosal glands of nasal turbinates from CFTR−/− and CFTR (DeltaF508/DeltaF508) pigs, *PLoS One*, 2011, **6**(8), e24424.
57 J. Y. Choi, *et al.*, Synergistic airway gland mucus secretion in response to vasoactive intestinal peptide and carbachol is lost in cystic fibrosis, *J. Clin. Invest.*, 2007, **117**(10), 3118–3127.
58 B. Meyrick, J. M. Sturgess and L. Reid, A reconstruction of the duct system and secretory tubules of the human bronchial submucosal gland, *Thorax*, 1969, **24**(6), 729.
59 J. L. Mummery, J. Killey and P. Linsdell, Expression of the chloride channel CLC-K in human airway epithelial cells, *Can. J. Physiol. Pharmacol.*, 2005, **83**(12), 1123–1128.
60 V. S. Shah, *et al.*, Airway acidification initiates host defense abnormalities in cystic fibrosis mice, *Science*, 2016, **351**(6272), 503–507.
61 X. X. Tang, *et al.*, Acidic pH increases airway surface liquid viscosity in cystic fibrosis, *J. Clin. Invest.*, 2016, **126**(3), 879–891.
62 X. Luan, *et al.*, Pseudomonas aeruginosa triggers CFTR-mediated airway surface liquid secretion in swine trachea, *Proc. Natl. Acad. Sci. U. S. A.*, 2014, **111**(35), 12930–12935.
63 R. Tarran, *et al.*, Regulation of murine airway surface liquid volume by CFTR and Ca2+–activated Cl- conductances, *J. Gen. Physiol.*, 2002, **120**(3), 407–418.
64 J. F. Collawn and S. Matalon, CFTR and lung homeostasis, *Am. J. Physiol.*, 2014, **307**(12), L917–L923.
65 X. Sun, *et al.*, Disease phenotype of a ferret CFTR-knockout model of cystic fibrosis, *J. Clin. Invest.*, 2010, **120**(9), 3149–3160.
66 X. Sun, *et al.*, In utero and postnatal VX-770 administration rescues multiorgan disease in a ferret model of cystic fibrosis, *Sci. Transl. Med.*, 2019, **11**(485), eaau7531.

